Metallography, Microstructure, and Analysis
https://doi.org/10.1007/s13632-018-0465-y

TECHNICAL ARTICLE

Friction Stir Welding of AlSi10Mg Plates Produced by Selective Laser Melting

Fabio Scherillo[1] · Antonello Astarita[1] · Umberto Prisco[1] · Vincenzo Contaldi[1,2] · Paolo di Petta[2] · Antonio Langella[1] · Antonino Squillace[1]

Received: 10 April 2018 / Revised: 8 June 2018 / Accepted: 20 June 2018

Abstract
A preliminary research work is carried out to demonstrate the feasibility of friction stir welding of AlSi10Mg plates produced by selective laser melting. The metallurgical evolutions occurring have been studied and discussed on the basis of detailed microstructure observations. The FSW process enhances the structure of the parent material so that the weld presents an overall refinement of the microstructure and a decrease in microporosity in all its zones. Using the friction stir welding technology, sound welds harder than the parent material can be obtained.

Keywords Friction stir welding · Selective laser melting · Microstructure · Hardness

Introduction

Additive layer manufacturing (ALM) is a production technology belonging to the field of additive manufacturing process. ALM employs a power source to produce a component by means of melting or sintering powders [1–3]. This manufacturing technology allows an efficient use of the raw materials resulting in minimal waste while reaching satisfactory geometric accuracy [4, 5].

In particular, starting from a digital 3D model, ALM produces parts by depositing material layer by layer. This manufacturing approach eliminates most of the constraints that hinder optimal design and creativity. Furthermore, it allows for the fabrication of complex and multi-functional material parts. Selective laser melting (SLM) is one of the ALM techniques that can be used to produce components with very complex internal structures. In addition, the as-build parts show a relatively smooth surface, so that they can be directly used without significant post-processing.

✉ Antonello Astarita
antonello.astarita@unina.it

[1] Department of Chemical, Materials and Production Engineering, University of Napoli Federico II, Piazzale Tecchio 80, 80125 Naples, Italy

[2] MBDA Italia, Via Calosi 105, 80070 Bacoli, Italy

However, there are many obstacles that still hamper the widespread adoption of metal-based ALM as a mainstream manufacturing method [6]. Among others, these include problems with the part quality, the process repeatability, the residual stresses, the internal porosities, and the low fatigue life compared to traditionally produced components, [7]. One of the major drawbacks for the wide application of SLM as an industrial processing route is the limited size of the products. This is a direct consequence of the limited dimensions of the available building chambers, which usually allows the production of samples with volumes of about 0.02 m^3. A possible way to overcome this problem would be the use of welding processes to join small SLMed objects to form larger parts.

In recent years, a number of studies have been focused on SLM, in particular on the optimization of the processing parameters and of the produced microstructures [8, 9]. However, to the best of authors' knowledge, there have been few investigations so far on the welding of components manufactures by SLM. In a previous paper, the joining of SLM-produced Al–12Si parts by the friction welding was studied [10], and other authors studied the joining of SLM-produced AlSi10Mg parts by electron beam welding process [11]. Friction stir welding (FSW) of aluminum alloys is widely studied in the literature, and several papers are available. The most important works are, however, mainly focused on FSW of alloys fabricated via

Published online: 03 July 2018

traditional process routes; see the important review on the subject by Mishraa and Ma [12] and the book: Mishra and Mahoney [13]. To date, there are no papers which study the frictions stir welding process of additive manufactured sheets. In this paper, the friction stir welding of AlSi10 plates produced by SLM is studied; in particular, the peculiar microstructure of the joints is discussed in detail.

Experimental

A near eutectic casting alloy, AlSi10Mg, whose composition is shown in Table 1, was used for the SLM process; the powder morphology was spherical. Only virgin powder was used, i.e., unused powder from a single powder lot. The size ranges within 40–71 μm, as measured using laser diffraction in accordance with ISO 13320-1. Figure 1 reports the histogram of the powder size distribution; particle diameters corresponding to 10, 50 and 90% of the size cumulative distribution were 49, 56 and 61 μm, respectively. The material's theoretical bulk density is 2.67 g/cm^3.

Several parallelepiped samples with a dimension of 20 × 20 × 4 mm were produced by SLM. The specimens were built using an EOSINT M 280 devise (EOS Group) equipped with a 250 × 250 × 300 mm building platform and an up to 400 W continuous Yb-fiber laser. The spot size of the laser was about 100 μm in diameter. The applied scanning velocity was 1 m/s. A single melt continuous scanning strategy was used with a scan spacing of 80 μm. Layer thickness prior to melting was 0.1 mm; scan orientation was turned by 90° at each layer. The laser operated at 180 W under an argon atmosphere with maximal oxygen content of 0.12%. The building direction of the SLM specimens was perpendicular to the 20 × 4-mm support base. The build platform was preset to a temperature of 150 °C before laser initialization.

Table 1 Chemical composition of the investigated AlSi10Mg alloy (wt.%)

Al	Balance
Si	10
Mg	0.35
Fe	0.14
Zn	0.02
Ti	0.01
Cu	0.02
Mn	0.02

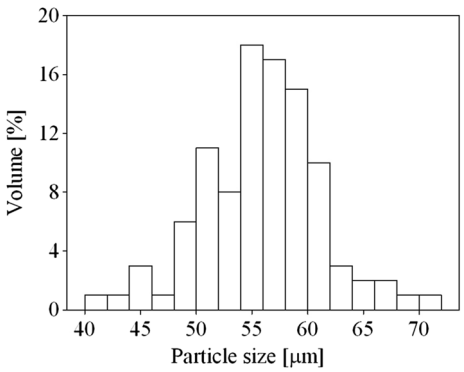

Fig. 1 Size distribution of the used powder

Subsequently, the plates were joined by FSW in butt configuration. Prior to welding, to ensure a smooth contact between the parts to be welded, 0.5 mm of material was removed from all the surfaces of the plates by milling. The involved surfaces were then cleaned by acetone washing and polished with abrasive paper to remove oxidation films and other impurities. A high-speed steel rotating tool with a cylindrical pin was used for the welding. The welding tool axis was perpendicular to the growth direction of the SLMed plates, while the welding direction was parallel to the 20 mm side of the base which was used as support for the plates during the SLM process. The tool is characterized by a shoulder diameter of 9 mm, pin diameter of 5 mm and pin length of 2.6 mm. The FSW was performed at a rotational speed of 900 rpm and at an advancing speed of 120 mm/min.

The relative density of the SLMed AlSi10Mg was measured by Archimedes' method weighting coupons extracted by the plates in ethanol and air, respectively. The specimens for optical microscopy of the weld zone were prepared using standard metallographic techniques. Transverse sections extracted perpendicularly to the welding direction were firstly encapsulated into epoxy and then accurately polished using a rotary grinder operating at 900 rpm. SiC papers from 200 down to 2000 and polishing fabrics with colloidal silica suspension were used. After polishing, to observe the microstructure of the weld zone, the surface was etched using the Keller's reagent (1.0 ml HF, 1.5 ml HCL, 2.5 ml HNO3, and 95 ml H_2O). Observations were carried out using an optical microscope and a Hitachi TM3000 scanning electron microscope operating at 40 keV in backscattered electron mode. EDX analysis at 15 keV was used to detect and map the element distribution within the different phases. Furthermore, with the aim of providing localized information about the elemental distribution, the electron beam was kept stationary on several spots of the samples to generate spectra of the different features of the material. In the adopted scanning conditions, the EDX spot size was estimated to be 0.1 μm with an excited volume of ∼ 1 μm^3. All the microscope images are taken in a plane parallel to the building direction and perpendicular to the welding direction. Vickers microhardness measurements were taken at the centerline on the cross section of the five specimens sliced from the

welds. The test load was 0.2 kg for 10 s. The test spacing between adjacent indentations was 0.4 mm.

Results and Discussion

The relative density of the SLM material was calculated to range between 94–95% with a porosity of about 5.2%. This value of the porosity is the expected one with the scan strategy used during the SLM process, whereas other strategies, as the single cross melt with random rotations of the hatch between the layers, are known to be able to reduce the porosity down to values equal to 1–2% [14].

A macrograph showing the entire structure of the weld is reported in Fig. 2.

The weld presents the classical morphology observed in friction-stir-welded butt joints [15]. This texture results from the intense plastic deformation and the exposure to high temperatures during the FSW. The weld zone becomes wider toward the upper surface because of the larger heating generated by friction and plastic flow below the shoulder. Based on the microstructural features of grains and precipitates, two distinct zones, namely the stirred zone (nugget) and the thermo-mechanically affected zone (TMAZ), can be identified within the weld. The microstructure of the parent material (PM) can be seen on the sides of the weld.

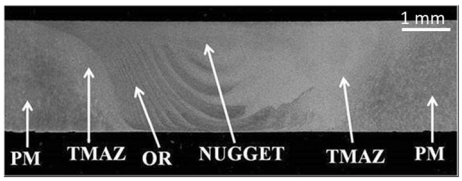

Fig. 2 Macrograph of the weld structure: parent material (PM), thermo-mechanically affected zone (TMAZ), onion rings (OR)

SEM microscopy reveals the so-called fish scale morphology with scales arranged in lines perpendicular to the laser beam direction in the cross section of the parent material (see Fig. 3a). Each scale represents the cross section of a distinct track of the laser beam: This is typical of SLM macrostructures [16–18]. Indeed, along the pass of the laser beam, the powder forms small melt pools which solidify rapidly. The melt pools have a half-cylindrical cross section with dimensions depending on the laser power and scan spacing and also on the scanning strategy. Considering that the melting occurs along the laser beam traces in each layer, the resulting microstructure is the consequence of this superposition of tracks. The structure shown in Fig. 3a arises from this directional growth. Inherent process defects, mostly pores, can be detected at low, Fig. 3a, and at high magnification, Fig. 3b. The porosity areal fraction is consistent with the calculated relative density. Both irregular and spherical pores are detected. The former, characterized by a maximum dimension of 25 μm, are located at the boundaries of the

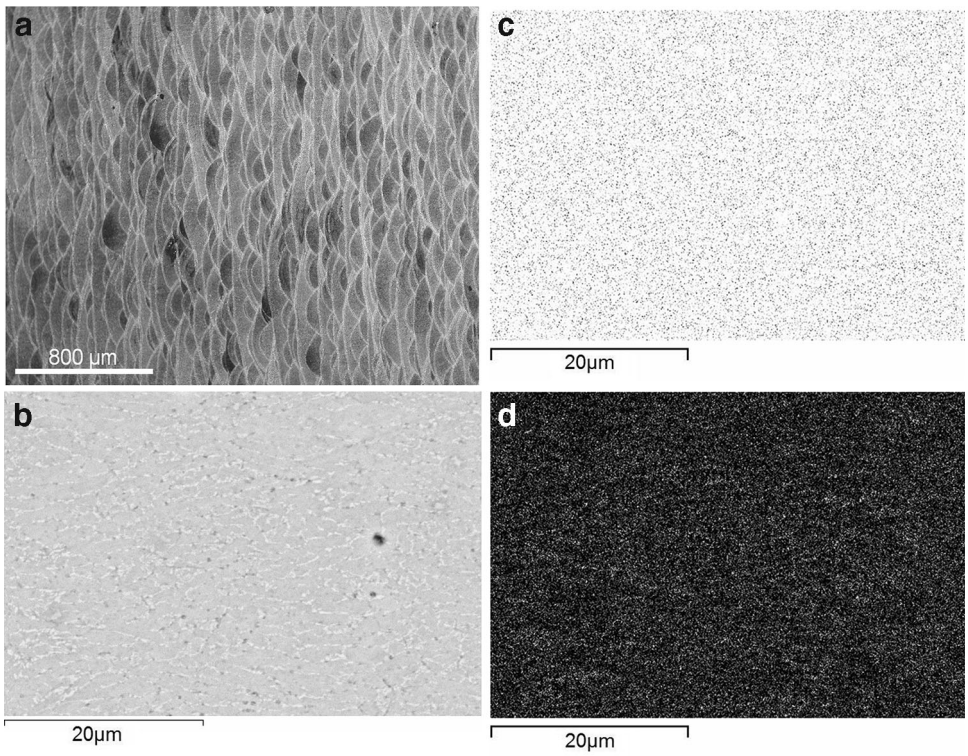

Fig. 3 SEM micrograph of the parent material at (**a**) low and (**b**) at high magnification (the growth direction is horizontal). EDX composition maps of the area in Fig. 3b: (**c**) Al (**d**) Si (the mapped element is in white)

melt pools; the most probable causes are unmelted particles or insufficient overlapping between adjacent scan traces. The latter, of a maximum dimension equal to 1 μm, are located within the melt pools and are caused by entrapped gasses.

Due to the extremely fast and layer-by-layer directional cooling of the small melt pools, the resulting microstructure is made up by very fine cellular dendrites with an average size about 3 μm (Fig. 3b). The formation of the very small cells can be easily understood considering the steep thermal gradient formed into the melting pool, on the order of 10^6 K/m according to the previous literature [19]. Gray cellular dendrites of the primary α-Al matrix are surrounded by interdendritic particles of the Si-rich phase, which appear as a white fibrous network at the grain boundaries. It is known that the fine dispersion of fibrous Si networks has a positive effect on the mechanical properties of the SLMed AlSi10Mg [20]. It is interesting to note that the fibrous network is somewhere interrupted by coarsening of the Si into idiomorphic particles. In conclusion, due to the peculiar porosity distribution and phase morphology, the final microstructure is characterized by a pattern of layer lines perpendicular to the laser beam and reflecting the layer-by-layer building of the material.

These observations are corroborated by the EDX composition maps of Fig. 3c and d. The maps show a fairly even distribution of Al in the sample, while the Si seems to be more confined in the regions corresponding to the white features of Fig. 3b. The punctual EDX spectra in Fig. 4 confirm that the white features located at grain boundaries are richer in Si. However, their composition is far from the equilibrium values due to the high cooling rate achieved during the SLM process with the consequent creation of a supersaturated Al matrix with a large content of Si (∼ 6 wt.%). EDX spectra integrated with stereological analyses based on the area fraction show that the weight fraction of the intergranular Si-rich phase is equal to ∼ 7%, which is not too far from the equilibrium value in a Al–Si alloy (∼ 10%).

The highly deformed structure of the TMAZ, located between the parent material and the nugget zone, is shown in Fig. 5a. Experiencing both high temperature and deformation, the TMAZ is characterized by a highly deformed structure with grains elongated in an upward flowing pattern and squeezed around the nugget zone by the forging action of the tool. Due to the insufficient deformation strain, recrystallization and grain coarsening do not occur in this zone. On the other hand, the micrograph in Fig. 5b shows that FSW probably had a beneficial effect in terms of homogenization and refinement of the microstructure. Indeed, the microstructure seems to have lost the pattern perpendicular to the building direction shown by the parent material. This can be attributed to a homogenization effect

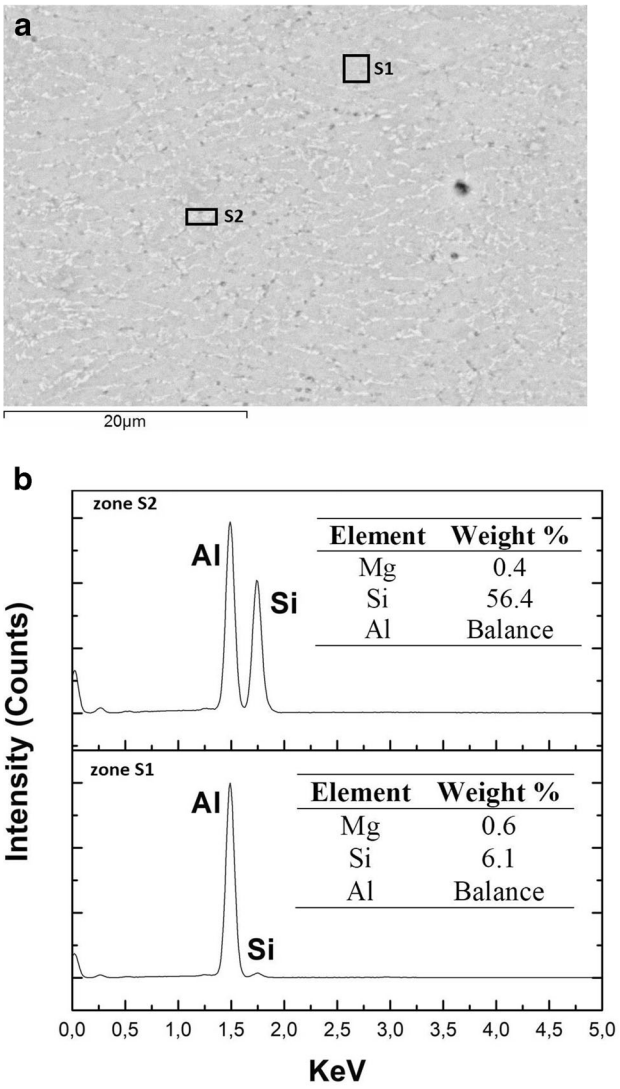

Fig. 4 EDX punctual spectra of different microstructural features in the parent material: (**a**) identification of the analyzed zones, (**b**) zone S1, α-Al matrix (gray), zone S2 phase layer rich in Si at the grain boundaries (white)

driven by the FSW tool which in addiction brought about a reduction of the porosity and a crushing of the Si-rich phase network surrounding the α-Al matrix. The Si-rich phase appears now much more evenly distributed and shows a more globular shape with dimensions slightly smaller than in the parent material. Furthermore, Fig. 5b reveals that the TMAZ contains a high-density of sub-boundaries on the contrary of the parent material.

Likewise, Du et al. [21] observed a reduction in porosity of AlSi10Mg specimens reinforced with carbon nanotubes fabricated by LSM and then friction stir processed. In the studied experiments, friction stir processing was able to significantly reduce the cavities present in selective laser melted composite and to uniformly disperse the carbon nanotubes in the aluminum matrix. Furthermore, the

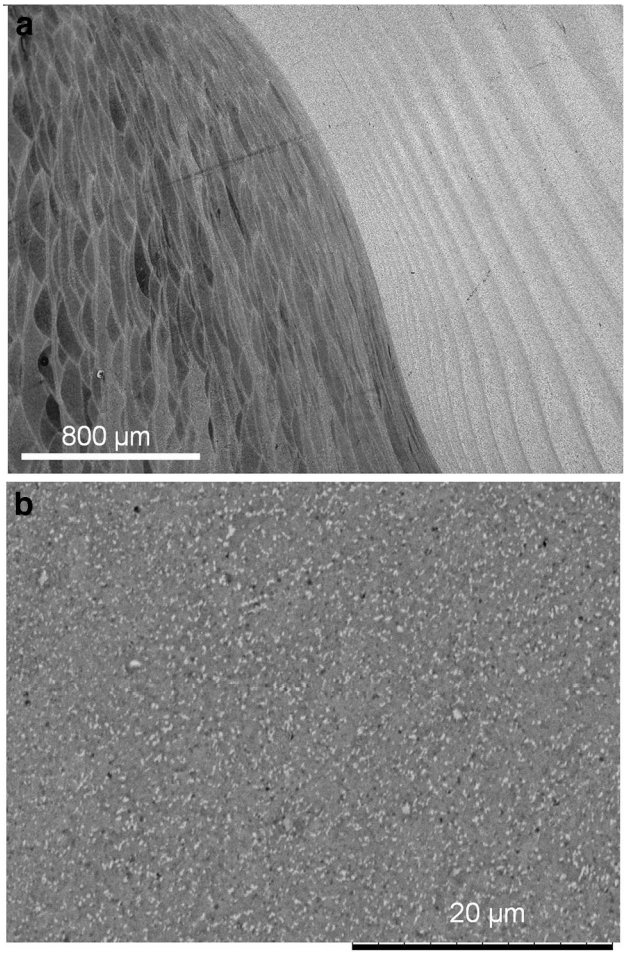

Fig. 5 (**a**) Micrograph of the boundary between the TMAZ and the OR; (**b**) micrograph of the TMAZ

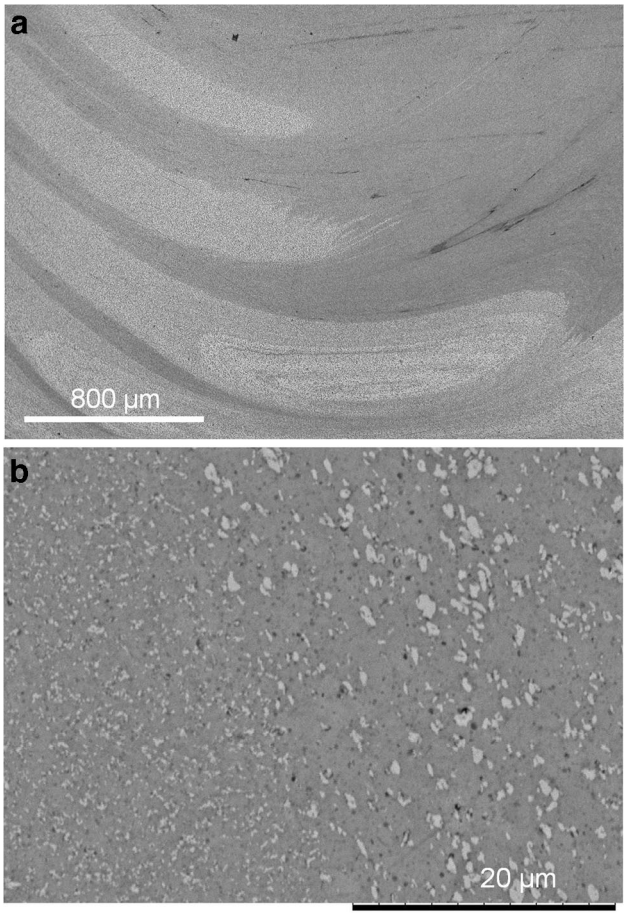

Fig. 6 Micrograph of (**a**) the nugget zone, (**b**) boundary between the nugget and the TMAZ

addition of carbon nanotubes resulted in relatively finer grains, effect mainly attributed by the authors to the Zener pinning effect.

The morphology of the nugget zone is reported in Fig. 6a. Its fine-grained microstructure is the result of the intense plastic deformation, frictional heating, and consequent dynamic recrystallization phenomena experienced by the material during the FSW. Onion ring structures are clearly observed; in particular, onion rings are more pronounced on the advancing side because plastic deformation is known to be more intense on this side of the weld. The closeup at the boundary between the nugget and the TMAZ in Fig. 6b reveals that the nugget has a finer microstructure than the TMAZ. Layer lines have completely disappeared while there is almost no trace of porosity. The nugget structure looks like a homogenous distribution of Si-rich phase, in the form of fairly globular particles, within an equiaxed aluminum matrix.

The distribution of Al and Si in the nugget was mapped using the EDX analysis (see Fig. 7). In comparison with the parent material, the Si seems now completely segregated in particular areas of the material, i.e., in the globular Si-rich phase. However, the Si-rich particles still contain Al; but now their Si content is increased to 78 wt.%. Likewise, the weight fraction of the globular Si-rich phase rose to $\sim$ 9%. Prashanth et al. [10] observed a similar result, although they friction-welded cylindrical rods produced by SLM of an Al–12Si powder. However, the change in weight fraction of free residual Si observed in their study was more drastic considering that it increased from 1 wt.% in the parent material to 10.5 wt.% in the weld zone. This difference is due to the higher level of supersaturation of the Al matrix of their parent material characterized by a very large content of Si ($\sim$ 11 wt.%). In turn, the supersaturation depends on the SLM process parameters which control the cooling rate, especially the power and the scanning speed adopted during the process. The size of the powder used can also play a key role in this regard.

The hardness profile across the weld, averaged over 5 specimens, is reported in Fig. 8. The mean values measured in each zone are in Table 2.

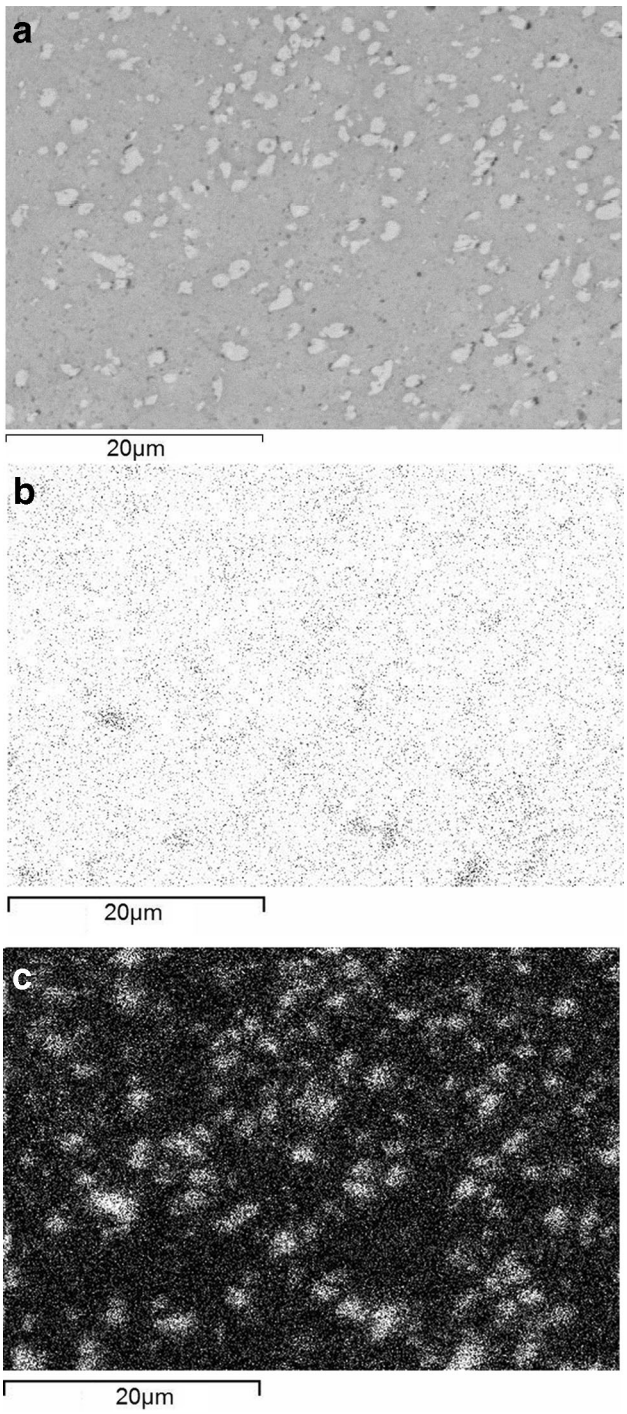

Fig. 7 (**a**) SEM micrograph from the core of the nugget; EDX composition maps: (**b**) Al, (**c**) Si (the mapped element is in white)

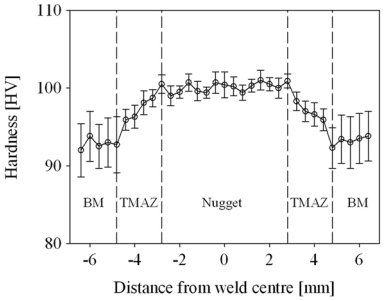

Fig. 8 Hardness profile measured across the weld (error bars represent the 68% confidence intervals)

Table 2 Hardness of the different zones of the weld (average values ± the standard deviation, corresponding to the 68% confidence intervals)

Zone	Hardness, HV
Parent material	93 ± 3
TMAZ	97 ± 1
Stirred zone	100 ± 1

The nugget is the hardest zone, with an average value of 100 HV. The hardness of the TMAZ, 98 HV, is also greater than that of the parent material, equal to 93 HV. On the contrary, Prashanth et al. [10] observed a softening of the nugget zone, which in their study shows a hardness lower than the parent material. In both cases, the parent material is a supersaturated Al matrix whose grains are surrounded by a network of a Si-rich phase. The matrix can then be considered as a solid-solution-hardened aluminum alloy. Generally, for this kind of alloy, FSW does not result in a softening of the welds, but rather in an increase in the hardness [12]. However, for the FW/FSW of SLM materials, two competing phenomena influence the final hardness of the nugget. On the one side, by decreasing the supersaturation of Si in the Al matrix and by destroying the Si network, FW/FSW tends to decrease the hardness of the weld. On the other side, FW/FSW increases the hardness with its usual action of grain refinement, porosity reduction, strain hardening, and by the dispersion strengthening due to the distribution of small particles. The parent material in [10] is a highly supersaturated Al matrix with a large content of Si ($\sim$ 11 wt.%) and, as consequence, it is very hard. The FW brings back the SLMed material to an equilibrium composition; this ends to be the main effect of the process resulting in a softening of the weld. In the case studied in this paper, the supersaturation level is lower ($\sim$ 6 wt.% of Si in the Al matrix) and the FSW is not able to completely bring back the parent material to the equilibrium condition. Then, the hardening phenomena prevail and the nugget shows an increase in the hardness. Nevertheless, the softening phenomena make their effect visible also in the presented study. The hardness increase of the nugget was only of $\sim$ 7 HV, while in cast alloys of this type increases as higher as $\sim$ 15 HV have been reported [10]. Finally, it is interesting to note that the homogenization performed by the FSW process brings about a reduction in the data dispersion for the nugget and the TMAZ; the standard deviation measured in these zones is indeed one-third of that of the parent material.

Conclusions

The results of this preliminary work show that selective-laser-melted AlSi10Mg plates can be successfully friction-stir-welded to produce larger parts. By breaking the layer-by-layer morphology resulting from the additive manufacturing process, the FSW process homogenizes the structure of the SLMed AlSi10Mg both macroscopically and microscopically. As a result, compared to the parent material, both the TMAZ and the nugget zone undergo a grain refinement and a decrease in porosity, with the nugget showing the larger effects. This enhances the weld hardness which reaches the maximum value in the stirred zone. Future researches need to focus on the mechanical properties of the welds, especially under fatigue, and on the relations between these properties and the building direction of the parent material.

Acknowledgments The authors are gratefully to FPT Industrie S.P.A. for its support to the experimental activity and for the preparation of the friction-stir-welded joints.

References

1. I. Gibson, D.W. Rosen, B. Stucker, *Additive Manufacturing Technologies: Rapid Prototyping to Direct Digital Manufacturing* (Springer, USA, 2009)
2. K.V. Wong, A. Hernandez, A review of additive manufacturing. Int. Sch. Res. Netw. **2012**, 1–12 (2012)
3. W.E. Frazier, Metal additive manufacturing: a review. J. Mater. Eng. Perform. **23**, 1917–1928 (2014)
4. ASTM, *Standard Terminology for Additive Manufacturing Technologies* (ASTM International, West Conshohocken, 2012)
5. G.N. Levy, R. Schindel, J.P. Kruth, Rapid manufacturing and rapid tooling with layer manufacturing (LM) technologies, state of the art and future perspectives. CIRP Ann. Manuf. Technol. **52**, 589–609 (2003)
6. L. Chauke, K. Mutombo, C. Kgomo, Characterization of the direct metal laser sintered Ti6Al4V components, in *14th Annual International RAPDASA Conference* (Free State, South Africa, 2013)
7. E. Sallica-Leva, A.L. Jardini, J.B. Fogagnolo, Microstructure and mechanical behavior of porous Ti–6Al–4V parts obtained by selective laser melting. J. Mech. Behav. Biomed. Mater. **26**, 98–108 (2013)
8. D.D. Gu, W. Meiners, K. Wissenbach, R. Poprawe, Laser additive manufacturing of metallic components: materials, processes and mechanisms. Int. Mater. Rev. **57**, 125–131 (2012)
9. L.E. Murr, S.A. Quinones, S.M. Gaytan, M.I. Lopez, A. Rodela, E.Y. Martinez, D.H. Hernandez, E. Martinez, F. Medina, R.B. Wicker, Microstructure and mechanical behavior of Ti–6Al–4V produced by rapid-layer manufacturing, for biomedical applications. J. Mech. Behav. Biomed. Mater. **2**, 20–32 (2009)
10. K.G. Prashanth, R. Damodaram, S. Scudino, Z. Wang, K. Prasad Rao, J. Eckert, Friction welding of Al–12Si parts produced by selective laser melting. Mater. Des. **57**, 632–637 (2014)
11. Moshe Nahmanya, Idan Rosenthal, Isgav Benishti, Nachum Frage, Adin Stern, Electron beam welding of AlSi10Mg workpieces produced by selected laser melting additive manufacturing technology. Addit. Manuf. **8**, 63–70 (2015)
12. R.S. Mishra, Z.Y. Ma, Friction stir welding and processing. Mater. Sci. Eng. R **50**, 1–78 (2005)
13. R.S. Mishra, M.W. Mahoney, *Friction Stir Welding and Processing* (ASM International, Materials Park, OH, 2007)
14. W. Pei, W. Zhengying, C. Zhen, D. Jun, H. Yuyang, L. Junfeng, Z. Yatong, The AlSi10Mg samples produced by selective laser melting: single track, densification, microstructure and mechanical behavior. Appl. Surf. Sci. **408**, 38–50 (2017)
15. C. Hamilton, S. Dymek, M. Blicharski, A model of material flow during friction stir welding. Mater. Charact. **59**, 1206–1214 (2008)
16. Lin-zhi Wang, Sen Wang, Wu Jiao-jiao, Experimental investigation on densification behavior and surface roughness of AlSi10Mg powders produced by selective laser melting. Opt. Laser Technol. **96**, 88–96 (2017)
17. E. Zaretsky, A. Stern, N. Frage, Dynamic response of AlSi10Mg alloy fabricated by selective laser melting. Mater. Sci. Eng. A **688**, 364–370 (2017)
18. D. Manfredi, F. Calignano, E.P. Ambrosio, M. Krishnan, R. Canali, S. Biamino, M. Pavese, E. Atzeni, L. Iuliano, P. Fino, C. Badini, From powders to dense metal parts: Characterization of a commercial AlSiMg alloy processed through direct metal laser sintering. Metall. Ital. **10**, 1–10 (2013)
19. Dong-Kyu Kim, Ji-Hyun Hwang, Eun-Young Kim, Yoon-Uk Heo, Wanchuck Woo, Shi-Hoon Choi, Evaluation of the stress-strain relationship of constituent phases in AlSi10Mg alloy produced by selective laser melting using crystal plasticity FEM. J. Alloys Compd. **714**, 687–697 (2017)
20. W. Li, S. Li, J. Liu, A. Zhang, Y. Zhou, Q. Wei, C. Yan, Y. Shi, Effect of heat treatment on AlSi10Mg alloy fabricated by selective laser melting: microstructure evolution, mechanical properties and fracture mechanism. Mater. Sci. Eng. A **663**, 116–125 (2016)
21. Z. Du, M.-J. Tan, J.F. Guo, J. Wei, C.K. Chua, Dispersion of CNTs in selective laser melting printed AlSi10Mg composites via friction stir processing. Mater. Sci. Forum **879**, 1915–1920 (2010)